Gas Processing Journal
Vol. 2, No.2, 2014
http://ijgs.ui.ac.ir/gpj

Investigating the Effects of Inlet Conditions and Nozzle Geometry on the Performance of Supersonic Separator Used for Natural Gas Dehumidification

S. H. Rajaee Shooshtari[1] , A. Shahsavand[2*]

Department of Chemical Engineering, Faculty of Engineering, Ferdowsi University of Mashhad, Mashhad, Iran

Abstract: Supersonic separators have found extensive applications in dehumidification of natural gases since 2003. Unlike previous studies, which have investigated the inlet conditions and nozzle geometry of supersonic separators for pure fluids, the present study employed a combination of momentum, heat, and mass transfer equations along with Virial equation of state (EOS) to inspect the effect of inlet conditions and nozzle geometry for methane-water systems. The simulation results were validated using several experimental data (borrowed from the literature) to ensure the capability of the current model. Afterward, the effects of various inlet parameters (P & T) and nozzle geometries (converging and diverging angles) were examined on the position of collection point and nucleation zone for separation of water vapor from a methane rich natural gas. The simulation results indicated that inlet gas temperature and pressure and diverging nozzle angle had severe effects on the condensation process inside supersonic separator, while the converging nozzle angle affects the inlet gas velocity and had minor effect on condensation process. For example, by increasing the 3S inlet pressure from 6 MPa to 10 MPa, the distance between throat and collection point reduced at least by half, whereas decreasing the inlet temperature from 300K to 285K, drastically decreased the same distance by fourth. The diverging nozzle angle effect approximately stood between the above two values.

Keywords: Supersonic Separator, Natural Gas, Dehumidification, Optimal Conditions, Geometry

1. Introduction

Supersonic separators have found extensive applications in oil and gas industries. Natural gas dehumidification, hydrocarbon dew point correction, CO_2 and H_2S removal, LPG extraction, and NGL separation from associated gases are only a few examples of such applications (Betting & Epsom, 2007). Moreover, solvent processing, use of membranes, adsorption and cryogenic separation can be used for separation and purification of natural gas from various impurities. These technologies require large facilities, high investment cost, and operating problems (Garmroodi Asil & Shahsavand, 2014; Gholami, Talaie, & Aghamiri, 2013; Mokhatab & Poe, 2012). Supersonic separators are suitable for separation of various impurities from natural gases because they create extremely cold conditions inside Laval nozzle which lead to condensations of almost all impurities from methane.

Laval nozzles are the main structural part of supersonic separators in all of its applications. In dehumidification process, the saturated gas enters into the plenum chamber with a relatively low velocity and high pressure at a reasonable temperature. As shown in Figure 1, a swirling motion is induced in the gas stream via a set of static vanes of the plenum chamber.

* Corresponding Author.

Authors' Email Address:
[1] Seyed Heydar Rajaee Shooshtari (s.h.rajaeeshooshtari@stu-mail.um.ac.ir), [2] Akbar Shahsavand (shahsavand@um.ac.ir)

ISSN (On line): 2345-4172, ISSN (Print): 2322-3251

The gas velocity increases to extremely high values (Ma>>1) when it passes through the diffuser section of the Laval nozzle. Consequently, the fluid pressure suddenly reduces due to the huge transformation of potential energy into kinetic energy. Moreover, the gas temperature dramatically drops across Laval nozzle because of the adiabatic expansion phenomenon. The combination of low temperature condition with strong swirling motion, created at supersonic velocity of the gas stream, results in efficient condensation and separation of water vapor (Vaziri, Shahsavand, Rashidi, & Mazidi, 2010).

As shown in Figure 2, the saturated gas initially enters the nozzle (section 1) and then expands to the sonic condition at the throat location (section 2). Evidently, the gas pressure and its corresponding temperature are drastically reduced as gas velocity increases. Hence, at a proper combination of pressure and temperature, the embryos of water droplets begin to form and grow as they enter section 3. The pressure reduction continues more intensely due to the nucleation process associated with these early embryos and the corresponding droplet growth for previously formed droplets. This area is known as nucleating zone and is terminated by the Wilson point (section 4). Downstream of Wilson point, nucleation ceases effectively and the number of droplets in the flow remains constant. Afterwards, the droplets grow rapidly and restore the system to thermodynamic equilibrium. If the amount of water vapor in the gas stream is sufficient, a sudden jump in pressure occurs due to the release of latent heat at supersonic conditions which tends to retard the supersonic flow. Further expansion of the flow takes place close to equilibrium conditions after section 5.

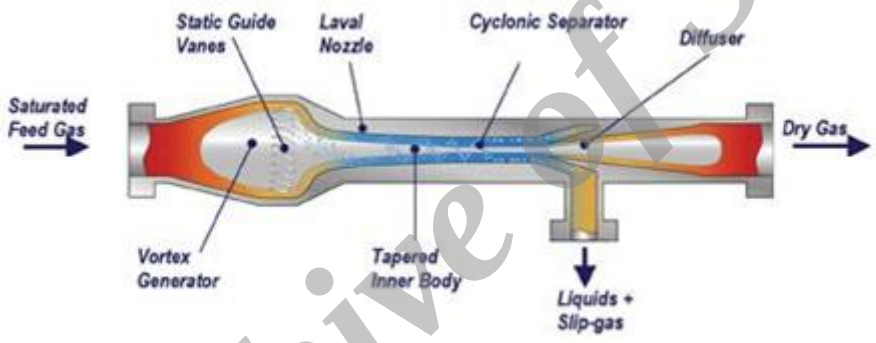

Figure 1. Schematic diagram of a supersonic separator

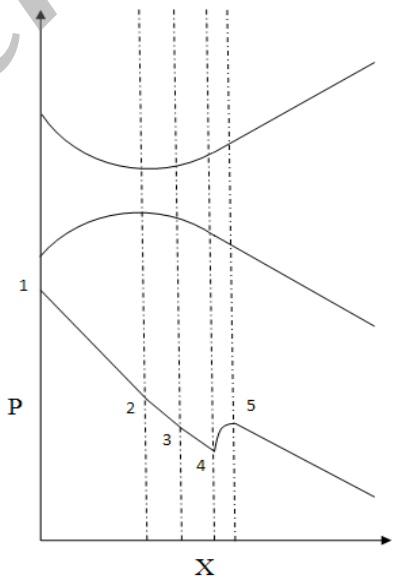

Figure 2. Axial pressure distribution in nozzle with condensation.

Most of the pervious theoretical works have investigated the effects of inlet conditions and operating parameters on single component and single phase flow inside supersonic separator without considering nucleation and growth processes.

Hengwei, Zhonggliang, Yongxun, Keyu, and Tingmin (2005) constructed a laboratory scale supersonic swirling system for natural gas dehydration. The corresponding inlet and outlet diameters of the 3S unit were 8 centimeters and its total length was about 1.5 meters. They used 2 humidity sensors at both 3S unit inlet and outlet and installed 9 thermocouples to monitor the temperature changes across the Laval nozzle. They obtained a maximum dew point temperature depression of around -20°C. Also, the effects of inlet temperature, gas flow rate, and pressure loss ratio on the dehydration characteristics were briefly analyzed. No experimental results were reported for condensation rate of water vapor from natural gas.

Jassim and colleagues used the CFD technique to examine the effects of real gas property, nozzle geometry, and vorticity on the performance of pure and single phase gases flowing inside Laval nozzle (2008a, 2008b). Their findings showed that shock wave position could significantly change when the gas was considered as real rather than perfect and although losses in pressure increased due to inlet swirl flow, but vorticity increased very sharply in the vicinity of the shock.

Karimi and Abdi investigated the influences of the inlet pressure, inlet temperature, and the exit back pressure on the normal shock-wave positions in supersonic nozzles (Karimi & Abdi, 2009) and reported that the normal shock wave occurred earlier by increasing the back pressure and decreasing the inlet temperature.

In 2011 and 2012, Wen et al. investigated the effects of the supersonic swirling flow on the radial distribution of the main parameters of gas flow inside 3S unit (Wen, Cao, & Yang, 2011; Wen, Cao, Yang, & Li, 2012; Wen, Cao, Yang, & Zhang, 2012). They also studied the effect of shock wave position, the particle trajectories, and separation efficiency by using the Discrete Particle Method (DPM).

Mahmoodzadeh Vaziri and Shahsavand examined the effects of various parameters (such as inlet pressure, temperature, velocity, pressure recovery, and outlet velocity) on geometry and dimensions of 3S unit predicted by a trained neural network (Vaziri & Shahsavand, 2013) and generated the training data were synthetically using a theoretical model. Most of these studies investigated the effects of various operating parameters on the overall performances of 3S unit, in absence of nucleation, growth and condensation phenomena.

Rajaee Shooshtari and Shahsavand proposed a new model based on multi-component nucleation and growth for modeling of 3S unit when no appreciable interaction existed between the condensed phases (Rajaee Shooshtari & Shahsavand, 2013). They showed that the model could provide reliable predictions for binary systems when only one component condensed.

The same approach will be used in the current article to investigate the effect of inlet conditions and nozzle geometries on the performance of 3S unit in dehumidification process. The effect of various inlet conditions and some nozzle geometries will be investigated on the position of nucleation zone, collection point, and separation efficiency of the entire dehumidification process.

2. Mathematical Model

By assuming steady state condition, the one dimensional governing equations for two-phase flow inside a converging-diverging nozzle can be expressed as a combination of continuity, momentum equation, energy equation, and other auxiliary relations.

2.1 Continuity:

The continuity equation for each desired section can be written as:

$$\dot{m}_t = \dot{m}_L + \rho_G A U_G \qquad (1)$$

Where $\dot{m}_t$ is the total mass flow rate, $\dot{m}_L$ is the liquid mass flow rate, ρ_G is the gas phase density, A is the cross-sectional area of nozzle at any segment and U_G is the gas velocity. Differentiating equation (1) for constant total mass rate and dividing the entire equation by gas flow rate ($\rho_G A U_G$) leads to:

$$\frac{d\rho_G}{\rho_G} + \frac{dA}{A} + \frac{dU_G}{U_G} + \frac{d\dot{m}_L}{\dot{m}_t - \dot{m}_L} = 0 \qquad (2)$$

2.2 Momentum Equation

The one dimensional momentum changes across each segment can be expressed as:

$$d\left[\dot{m}_G U_G + \dot{m}_L U_L\right] = -A dP - \frac{f A \rho_G U_G^2}{2 d_e} dx \qquad (3)$$

Where f is the friction factor and d_e is the hydraulic diameter. Assuming no slippage between the gas and liquid phases $(U_G = U_L)$ and dividing equation (3) by $(A \times P)$, the momentum equation can be simplified and rearranged as:

$$\frac{dP}{P} = -\frac{f \rho_G U_G^2}{2P}\frac{dx}{d_e} - \frac{m_t U_G}{AP}\frac{dU_G}{U_G} \qquad (4)$$

As before, the total mass flow rate is assumed to be constant and the second term in the right had side is multiplied and divided by U_G, to keep the previous trend.

2.3 Equation of state

The following second order Virial equation of state (EOS) can be written as:

$$P = \rho_G \hat{R} T_G (1 + B_1 \rho_G) \quad (5)$$

Where $\hat{R}$ is the universal gas constant on a mass basis and B_1 is the second viral coefficient. By differentiating equation (5) and using some mathematical manipulations, the following result will be achieved:

$$\frac{dP}{P} - X\frac{d\rho_G}{\rho_G} - Y\frac{dT_G}{T_G} = 0 \quad (6)$$

$$X = \frac{\rho_G}{P}\left(\frac{\partial P}{\partial \rho_G}\right)_{T_G} = \frac{1 + 2B_1\rho_G}{1 + B_1\rho_G}$$

$$Y = \frac{T_G}{P}\left(\frac{\partial P}{\partial T_G}\right)_{\rho_G} = 1 + \frac{\rho_G T_G}{1 + B_1\rho_G}\left(\frac{dB_1}{dT_G}\right)$$

2.4 Energy equation

Assuming the small heat loss at any section, the energy equation for steady state flow can be written as:

$$d\left[\dot{m}_G\left(h_G + \frac{U_G^2}{2}\right) + \dot{m}_L\left(h_L + \frac{U_L^2}{2}\right)\right] = 0 \quad (7)$$

Where h_G and h_L are the gas and liquid enthalpies, respectively. The change of enthalpy of the vapor phase can be expressed by:

$$dh_G = \left(\frac{\partial h_G}{\partial T_G}\right)_P dT_G + \left(\frac{\partial h_G}{\partial P}\right)_{T_G}$$

$$dP = c_P dT_G + \left[V_G - T_G\left(\frac{\partial V_G}{\partial T_G}\right)_P\right] \quad (8)$$

$$dP = c_P dT_G + \frac{1}{\rho_G}\left(1 - \frac{Y}{X}\right)$$

Dividing equation (7) by $\dot{m}_t c_p T_G$ and replacing latent heat $(h_G - h_L)$ with h_{fg} leads to the following equation.

$$\frac{dT_G}{T_G} + \frac{P}{\rho_G c_p T_G}\left(1 - \frac{Y}{X}\right)\frac{dP}{P} + \frac{U_G^2}{c_p T_G}\frac{dU_G}{U_G} - \frac{h_{fg}}{C_p T_G}\frac{d\dot{m}_L}{\dot{m}_t} = 0 \quad (9)$$

2.5 Mach Number

Square of Mach number equation can be expressed as:

$$Ma^2 = \frac{U_G^2}{\gamma P / \rho_G} \quad (10)$$

Where γ is the ratio of specific heats. Differentiating equation (10) leads to:

$$\frac{d(Ma^2)}{(Ma^2)} = 2\frac{dU_G}{U_G} + \frac{d\rho_G}{\rho_G} - \frac{dP}{P} \quad (11)$$

2.6. Liquid mass flow rate:

Liquid mass flow rate at each increment can be calculated by computing the nucleation and growth rates.

2.6.1. Nucleation rate

The rate of formation of critical droplets per unit volume and time can be calculated from classical nucleation theory (McDonald, 1962).

$$J = \frac{q_c}{1+\eta}\frac{\rho_{wv}^2}{\rho_L}\sqrt{\frac{2\sigma_{wv}}{\pi m_{wv}}}\exp\left(-\frac{4\pi r^{*2}\sigma_{wv}}{3kT_G}\right) \quad (12)$$

Where J is nucleation rate, q_c is the condensation coefficient, σ is the surface tension, m is mass of single molecule, k is the Boltzmann constant (1.3807×10^{-23} J/K) and subscripts wv and L indicate the water vapor and liquid, respectively. r^* and η are the critical radius and non-isothermal correction and can be calculated from following correlation:

$$r^* = \frac{2\sigma_{wv}}{\rho_L R T_G \ln S_{wv}} \approx \frac{2\sigma_{wv} T^{sat}(P_{wv})}{\rho_L h_{fg}(T_G - T^{sat}(P_{wv}))} \quad (13)$$

$$\eta = \frac{2(\gamma-1)}{1+\gamma}\frac{h_{fg}}{RT_G}\left(\frac{h_{fg}}{RT_G} - 0.5\right) \quad (14)$$

Where S is the super-saturation ratio, $T^{sat}(P_{wv})$ is the saturation temperature at partial pressure of water vapor and γ is the specific heat capacity ratio.

2.6.2 Growth rate

Liquid droplet growth can be calculated from following equation (Rajaee Shooshtari & Shahsavand, 2013):

$$\frac{dR_d}{dt} = \frac{DM_{wv}}{\rho_L}\frac{\sqrt{\pi Dt} + R_d}{R_d\sqrt{\pi Dt}}\left(\frac{Py_{wv}}{z(T_G, P)RT_G} - \frac{P^{sat}(T_L)}{z(T_L, P^{sat})RT_L}\right) \quad (15)$$

Where R_d is the droplet radius, D is diffusion coefficient, M is the molecular weight, y is water vapor mole fraction in the bulk and superscript *sat* indicates the saturation state.

Liquid mass generation rate at each segment (j) can be calculated from the following relation:

$$\dot{m}_{Lsegj} = \left(4/3\pi r_j^{*3}\rho_L J_j V_{segj}\right) + \left(4/3\pi\rho_L\left(\sum_{i=1}^{j-1} J_i V_{segi}\right)\left((R_d + dR_d)^3 - R_d^3\right)\right) \quad (16)$$

Ultimately, the total liquid mass flow rate at any segment (j) is given by the following equation:

$$\dot{m}_L = \sum_{i=1}^{j} \dot{m}_{Lsegi} \qquad (17)$$

The entire set of ordinary differential equations are solved in a stepwise manner using the in-house fourth order Runge-Kutta method. Initially, a set of temperature, pressure and gas density are assumed at the outlet of each incremental segment. Then the corresponding nucleation and growth rates along with the liquid mass flow are computed using appropriate equations. Finally the assumed valued are calculated via simultaneous solution of the fundamental governing equations and rechecked until convergence is established.

3. Model validation

The present model can be used for condensation of any condensable impurity from non-condensable gases. The experimental data of Wegener et al. for condensation of ethanol vapor from air stream in Laval nozzle (borrowed from Kumar and Levin), were used for model validation purposes (Kumar & Levin, 2011; Wegener, Clumpner, & Wu, 1972). Diffuser geometry is shown in Figure 3 and the corresponding experimental operating parameters are presented in Table 1. Table 2 provides all physical properties required for validation (Kumar & Levin, 2011; Perry, Green, & Maloney, 1997).

The present formulation described in the previous section was used with the throat conditions reported by Kumar and Levin to simulate the ethanol droplets growth rate inside the Laval nozzle of the 3S unit. Figure 4 compares the simulations results of the present theoretical model with the experimental data reported by Wegener et al for three different ethanol vapor mass fractions at inlet condition for a) variations of cluster to mixture fraction (mass of condensed ethanol to total mass) and b) mass fraction of condensed ethanol (relative to inlet condition) with dimensionless length (x/D), where D is the throat diameter. The impressive proximity of the experimental data and the model predictions illustrates that the present approach can be used as a powerful tool for modeling and design of Laval nozzle behavior in supersonic separator for separation of condensable species from non-condensable streams.

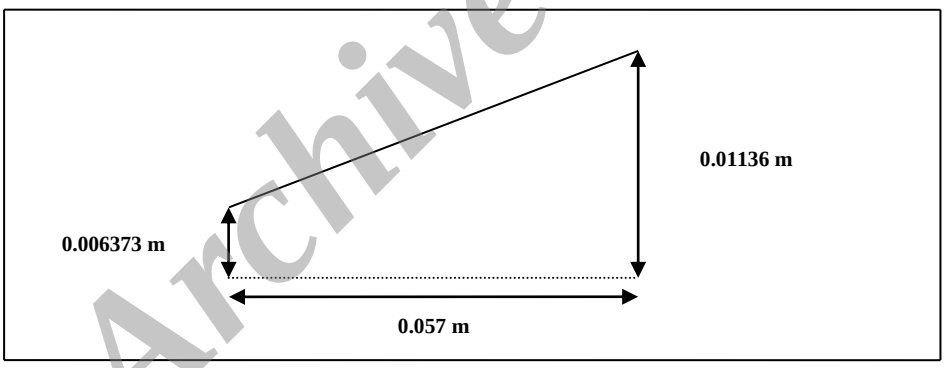

Figure 3. Geometry of diffuser section used in experimental data of Wegener et al (Wegener et al., 1972)

Table 1. Operating conditions used in experimental data of Wegener et al., (Wegener et al., 1972)

Prameter	Unit	Value
Stagnation pressure	Kpa	83.4
Stagnation temprature	K	296
Ethanol content at inlet	Mass fractions	0.0034, 0.005, 0.008
Throat pressure	Kpa	41.7
Throat temperature	K	248.64
Ethanol content at throat	Mass fractions	0.0034, 0.005, 0.008

Table 2. Ethanol physical properties required for validation.

Prameter	Unit	Value
Surface tension	J/m²	$0.001\times\left(23.97-0.085\left(T(K)-273.15\right)\right)$
Latent heat	J/kmol	$5.69\times10^{7}\times\left(1-T(K)/513.92\right)^{0.3359}$
Vapor pressure	Pa	$\exp(74.475-7164.3/T(K)-7.327\times\ln(T(K)+3.134\times10^{-6}\times T^{2})$
Liquid density	Kmol/m³	$1.648/0.27627^{(1+(1-T(K)/513.92)^{0.2331}}$
heat capacity	J/(kmol.K)	$1.0264\times10^{5}-1.3963\times10^{2}\times T(K)-3.0341\times10^{-2}\times T(K)^{2}+2.0386\times10^{-3}\times T(K)^{3}$
Molecular weight	kg/kmol	46.069

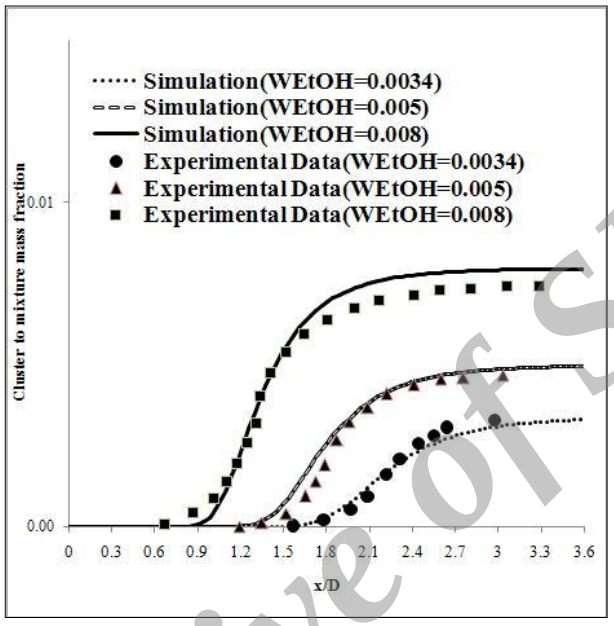

a) cluster to mixture fraction

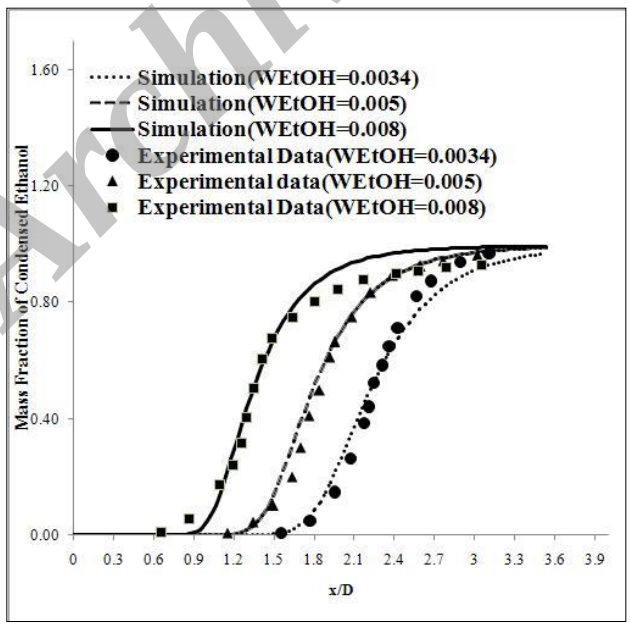

b) mass fraction of condensed ethanol

Figure 4. Comparison of simulation results with experimental data of Wegener et al. (Wegener et al., 1972)

4. Simulation results

The validated model will be used in this section to investigate the effects of inlet conditions and

nozzle geometry on the performance of supersonic separator employed for dehumidification of natural gas. Figure 5 provides the typical Laval nozzle geometry used for all simulations. The inlet gas composition and the corresponding domains of various inlet operating conditions are presented in Table 3. Inlet gas velocity depends on both the converging length (x_t) and converging angle (α). For each individual case the gas flow rate inside Laval nozzle was automatically adjusted to obtain unit Mach number at the throat location. As Mokhatab and Poe (2012) note, when 3S unit is used for dehumidification process, the collection point should be selected so that the amount of water vapor in the dry gas leaving the 3S unit becomes less than the permissible value of 7 lbm water / MMSCF natural gas.

4.1 Effects of inlet pressure and temperature

Figures 6a and 6b provide the effects of inlet pressure and inlet temperature on the overall nucleation process (both rate and position of nucleation occurrence). As it can be seen, the nucleation process occurred earlier at high inlet pressures and low inlet temperatures. Furthermore, increasing the inlet pressure or decreasing the inlet temperature drastically sharpened the nucleation curve and led to larger nucleation rates. By increasing the inlet pressure or decreasing the inlet temperature, the super-saturation ratio increases at the inlet condition and early nucleation will occur.
Evidently, for all of these pressures and temperatures, the amount of water vapor can be reduced to its permissible value but the position of the liquid collection point will be different for each individual case shown in Figure 7. The figure clearly shows that the position of liquid collection point moves away from the throat location when the inlet temperature is increased or the inlet pressure is decreased.

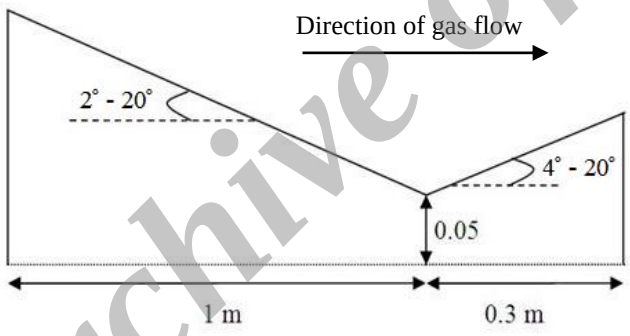

Figure 5: Typical nozzle geometry for dehumidification process

Table 3: Inlet compositions and domains of various operating conditions.

Prameter	Unit	Value
Methan mole fraction	mole fraction	0.9994
Water vapor mole fraction	mole fraction	0.0006
Inlet pressure range	MPa	6 – 10
Inlet temprature	K	285 – 300
Inlet velocity	m/s	3 – 83

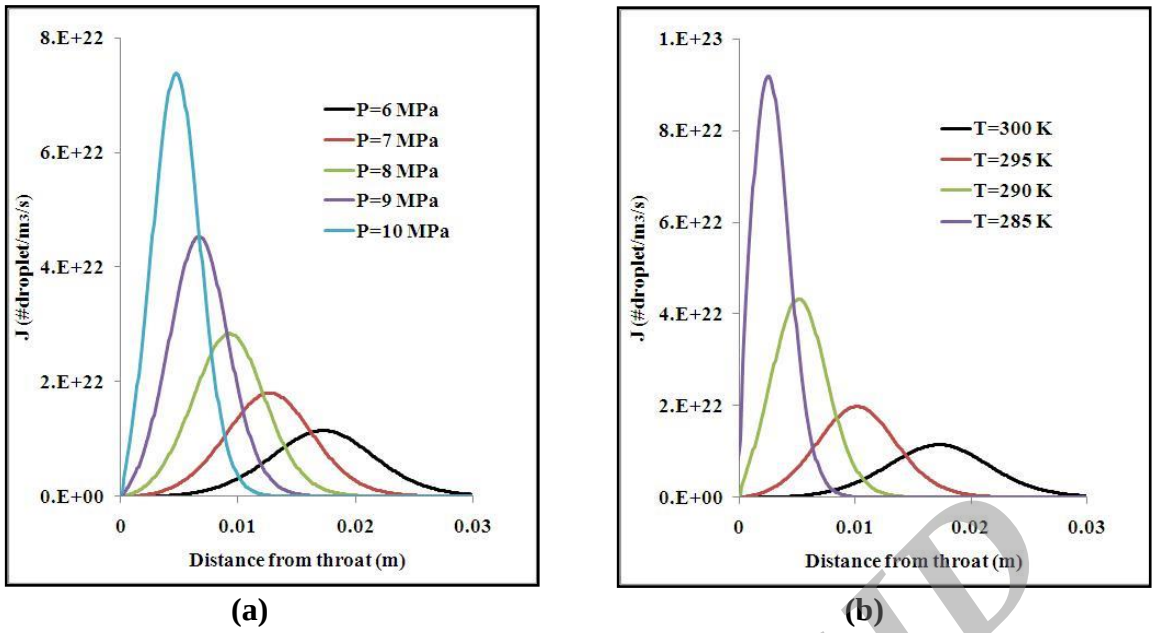

Figure 6: Effects of (a) inlet pressure at T= 300 K and (b) inlet temperature at P=6 MPa on nucleation curves (Inlet gas velocity is assumed to be 69 m/s for all cases).

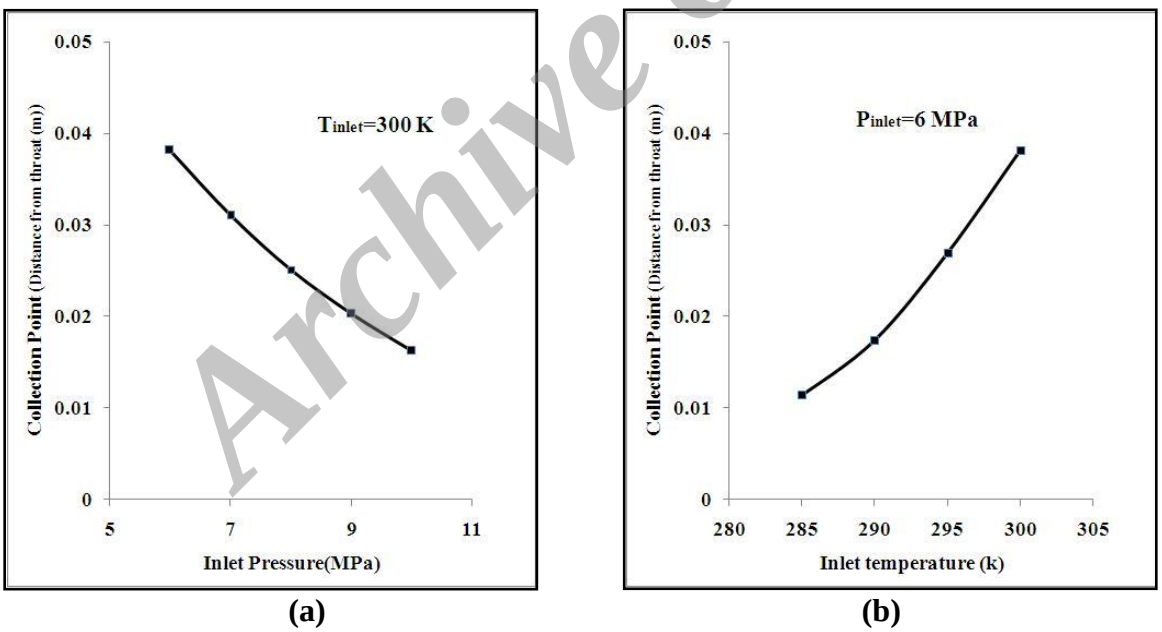

Figure 7: Effects of a) inlet pressure and b) inlet temperature on the collection point location.

In order to compare the effects of the temperature and pressure on the performance of 3S unit at the same condition, the inlet pressure versus the inlet temperature is

plotted in Figure 8, when the liquid collection point is located 0.02m* away from the throat. Several trials were made in each case to ensure that the water vapor content of the natural gas at collection point would be less than the standard value. This figure can be used to estimate the equivalent inlet pressure change of the ordinate which produces the same effect as the inlet temperature change of the abscissa. For example, increasing the inlet pressure from 6 MPa to 9 Mpa had the same effects when the inlet temperature decreased from 299.85 K to 291.5 K.

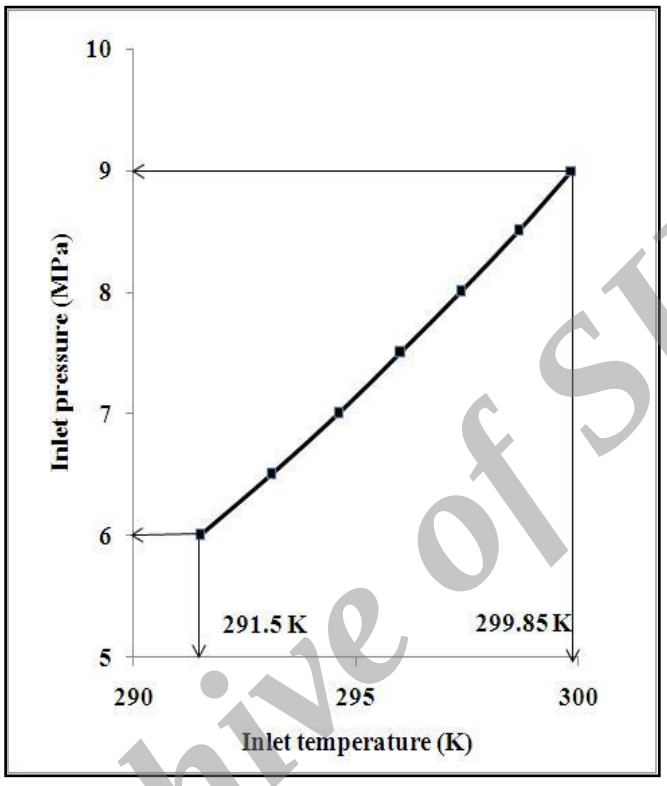

Figure 8: Inlet pressure versus inlet temperature for fixed position of collection point at x=0.02m(distance from throat)

* This value is selected such that both inlet temperature and inlet pressure remain in the previously specified range shown in Figure 8

4.2 Effects of Laval nozzle geometry

Obviously, Laval nozzles play a critical role in the structure of supersonic separators in

dehumidification process. Figures 9 to 12 illustrate the effects of various converging and diverging angles on the position of the collection points, the location of nucleation zone and the magnitude of inlet gas velocity. All runs were executed when the entire length of converging nozzle was kept constant at 1m and the inlet pressure and temperature were 6 MPa and 300K, respectively. As it can be seen, the converging angle has a minor effect on the position of collection point and the location of nucleation zone, because both of them occur in the diverging section of the Laval nozzle. On the other hand, the converging angle value has strong effect on inlet gas velocity as shown in Figure 10. This is because much sharper converging nozzle angles are required to create unit Mach number at the throat.

In contrast to converging angle, the diverging angle has immense effect on the structure and geometry of the 3S unit for a fixed performance. Figures 11a and 11b show that the position of both collection point and nucleation peak moves toward the throat as the diverging angle is decreased. Evidently, the required length for both diverging section and the entire length of 3S unit will be reduced as diverging angle is decreased.

Figure 12 clearly illustrates that the temperature reduction across 3S unit becomes more rapid as diverging angle is increased. Sharp decrease in gas temperature will certainly result early super-saturation and encourages both nucleation and growth processes. In practice, the separation phenomenon may occur at large diverging angles which change the entire temperature profile due to the non-isentropic behavior of the separation event.

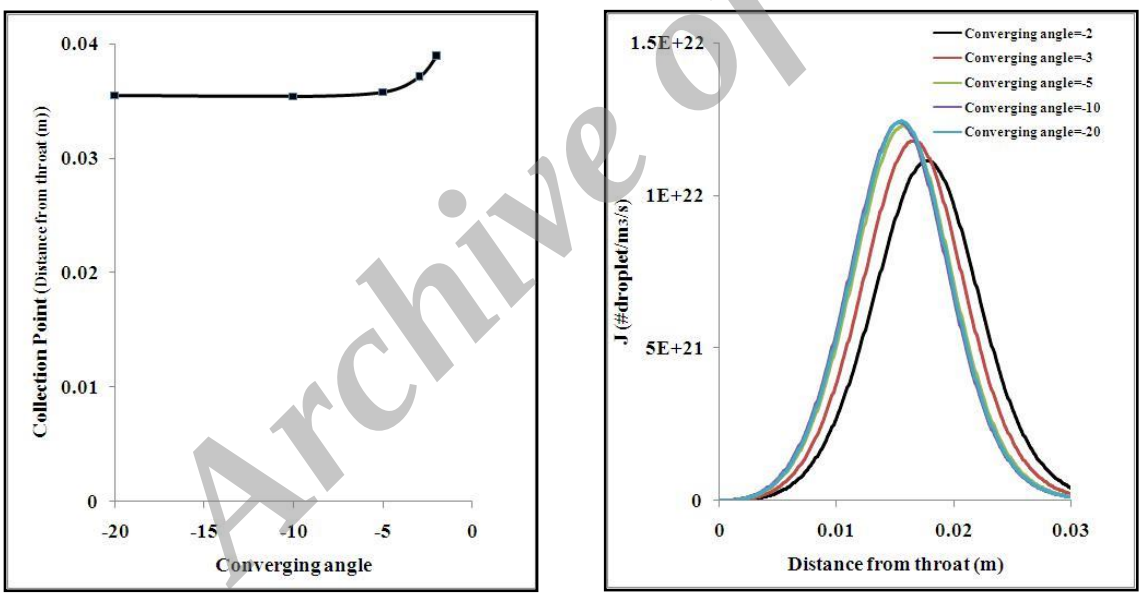

(a) **(b)**

Figure 9: Effects of converging angle on the location of
(a) collection point (b) nucleation zone

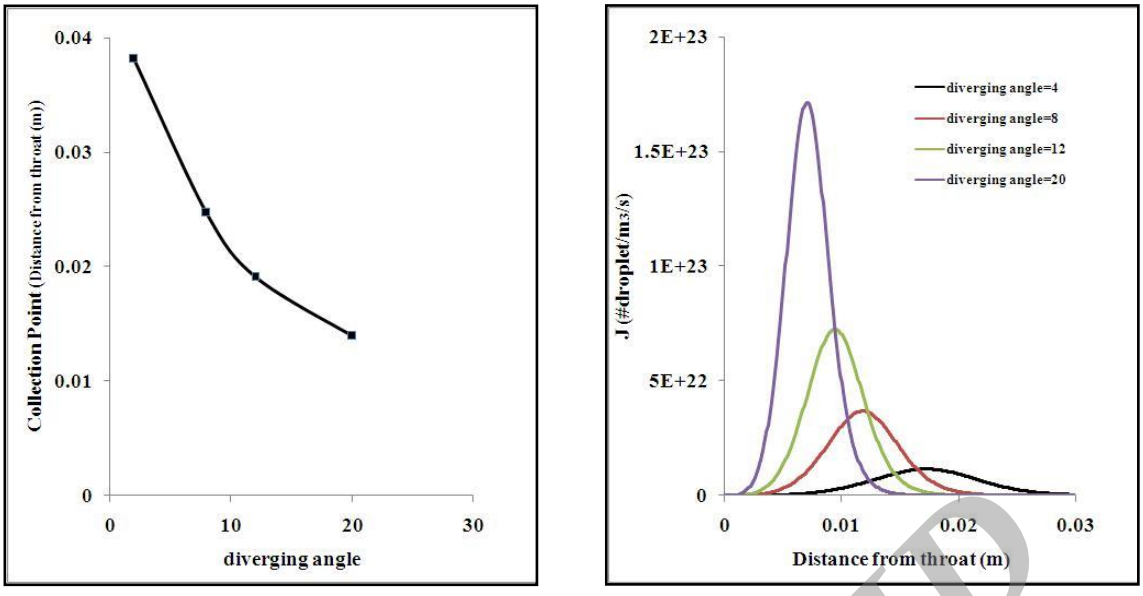

Figure 11. Effects of diverging angle on the location of (a) collection point (b) nucleation zone

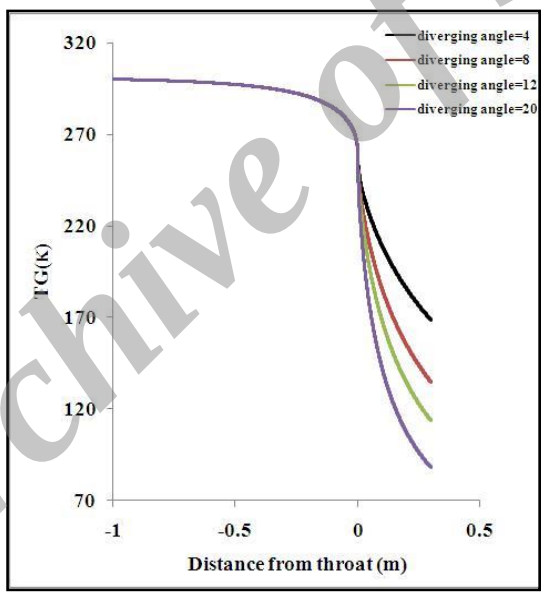

Figure 12. Effect of diverging angle on the temperature distribution

5. Conclusion

Natural gas dehumidification is the most important application of supersonic separators in oil and gas industries. Inlet conditions and

nozzle geometries have great effects on the droplet nucleation zone, position of the collection point, and process separation efficiency. Unlike previous studies, the present study investigated the performances of supersonic separators for dehumidification process when various operating conditions and nozzle geometries were used. The one-dimensional equations for compressible gas flow inside supersonic Laval nozzle was combined with multi-component nucleation and growth to modeling of dehumidification process via supersonic separators. The mathematical model was initially validated successfully with several experimental data and then the effect of various inlet pressures, inlet temperatures, converging and diverging angle were investigated on the position of collection point and nucleation zone. The simulation results indicated that while inlet gas temperature, inlet gas pressure, and diverging angle of the diffuser section had appreciable effects on the process efficiency, nucleation zone, position of liquid collection point, and performance of the supersonic separator, however, the converging angle of the Laval nozzle had minor effect on those parameters and only affected the inlet gas velocity. It was clearly found that increasing the inlet pressure from 6 MPa to 10 MPa, reduced the distance between throat and collection point at least by half. On the other hand, decreasing the inlet temperature from 300K to 285K, drastically reduced the same distance by fourth. Evidently, the temperature reduction had more dramatic effect than the pressure increase on the collection point location. In a similar manner, the diverging nozzle angle effect approximately stood between the above two values.

Nomenclature

A	Area (m^2)
B_1	Second virial coefficient
C_p	Specific heat at constant pressure (j kg^{-1} k^{-1})
D	Diffusion coefficient (m^2 s^{-1})
d_e	Hydraulic diameter (m)
f	Friction factor
h	Enthalpy (j kg^{-1})
h_{fg}	Latent heat (j kg^{-1})
J	Rate of formation of droplets per unit volume and time (# droplets m^{-3} s^{-1})
k	Boltzmann constant (1.3807×10^{-23} J/K)
m	Mass of single molecule (kg)
M	Molecular weight (kg $kgmol^{-1}$)
Ma	Mach number
$\dot{m}$	Mass flow rate (kg s^{-1})
P	Pressure (Pa)
$T^{sat}(P)$	Saturation temperature at p (k)
q_c	Condensation coefficient
$\hat{R}$	Universal gas constant on a mass basis (j kg^{-1} k)
r^*	Critical radius
R_d	Mean droplet radius (m)
S	Super-saturation ratio
T	Temperature (k)
U	Velocity (m s^{-1})
V_{segj}	Volume of segment j (m^3)
WEtOH	Mass fraction of ethanol
X	Function of temperature and density in equation of state
Y	Function of temperature and density in equation of state
γ	Specific heat capacity ratio
ρ	Density (kg m^{-3})
σ	Surface tension (j m^{-2})
η	Non-isothermal correction factor

Subscripts

G	Vapor phase
L	Liquid phase
t	Total
wv	Water vapor

Superscripts

*	Critical
sat	Saturation

References

Betting, M., & Epsom, H. (2007). Supersonic comparator gains market acceptance. *World Oil*, *228*(4): 197–200.

Garmroodi Asil, A., & Shahsavand, A. (2014). Selecting Optimal Acid Gas Enrichment Configuration For Khangiran Natural Gas Refinery. *Gas Processing*, *2*(2), 1–21.

Gholami, M., Talaie, M. R., & Aghamiri, F. (2013). Investigating the Performance of Amine-Grafted Silica-Base Adsorbents in CO2 Removal from a Natural Gas Stream Using a Diffusion Based Mathematical Model. *Gas Processing Journal*, *1*(2): 22–30.

Hengwei, L., Zhonggliang, L., Yongxun, F., Keyu, G., & Tingmin, Y. (2005). Characteristic of a supersonic swirling dehydration system of natural gas. *Chinese Journal of Chemical Eng*, *13*(1), 9–12.

Jassim, E., Abdi, M. A., & Muzychka, Y. (2008a). Computational fluid dynamics study for flow of natural gas through high-pressure supersonic nozzles: part 2. Nozzle geometry and vorticity. *Petroleum*

Science and Technology, 26(15), 1773–1785.

Jassim, E., Abdi, M. A., & Muzychka, Y. (2008b). Computational fluid dynamics study for flow of natural gas through high-pressure supersonic nozzles: Part 1. Real gas effects and shockwave. *Petroleum Science and Technology, 26*(15): 1757–1772.

Karimi, A., & Abdi, M. A. (2009). Selective dehydration of high-pressure natural gas using supersonic nozzles. *Chemical Engineering and Processing: Process Intensification*, *48*(1), 560–568.

Kumar, R., & Levin, D. A. (2011). Simulation of homogeneous condensation of small polyatomic systems in high pressure supersonic nozzle flows using Bhatnagar–Gross–Krook model. The *Journal of chemical physics, 134*(12), 124519.

McDonald, J. E. (1962). Homogeneous nucleation of vapor condensation. I. Thermodynamic aspects. *Am. J. Phys, 30*(12), 870–877.

Mokhatab, S., & Poe, W. A. (2012). *Handbook of natural gas transmission and processing*. Gulf Professional Publishing.

Perry, R. H., Green, D. W., & Maloney, J. O. (1997). *Perry's chemical engineers' handbook*. McGraw-hill, New York.

Rajaee Shooshtari, S., & Shahsavand, A. (2013). Reliable prediction of condensation rates for purification of natural gas via supersonic separators. *Separation and Purification Technology, 116*, 458–470.

Vaziri, B., Shahsavand, A., Rashidi, H., & Mazidi, M. (2010). *Non isentropic performance of supersonic separators*. Paper presented at the 13th Iranian National Chemical Engineering Congress and 1st International Regional Chemical and Petroleum Engineering Kermanshah, Iran.

Vaziri, B. M., & Shahsavand, A. (2013). Analysis of supersonic separators geometry using generalized radial basis function (GRBF) artificial neural networks. *Journal of Natural Gas Science and Engineering, 13*, 30–41.

Wegener, P. P., Clumpner, J. A., & Wu, B. J. (1972). Homogeneous nucleation and growth of ethanol drops in supersonic flow. *Physics of Fluids, 15*(11), 1869–1876.

Wen, C., Cao, X., & Yang, Y. 2011. Swirling flow of natural gas in supersonic separators. Chemical Engineering and Processing. *Process Intensification, 50*(7), 644–649.

Wen, C., Cao, X., Yang, Y., & Li, W. (2012). Numerical simulation of natural gas flows in diffusers for supersonic separators. *Energy, 37*(1), 195–200.

Wen, C., Cao, X., Yang, Y., & Zhang, J. (2012). Evaluation of natural gas dehydration in supersonic swirling separators applying the Discrete Particle Method. *Advanced Powder Technology*, *23*, 228–233.